Stabilizing single atoms and a lower oxidation state of Cu by a ½[110]{100} edge dislocation in Cu-CeO_{2}

Lixin Sun and Bilge Yildiz

Stabilizing single atoms and lower oxidation state of Cu by an ½[110]{100} edge dislocation in Cu-CeO₂

Lixin Sun,[1] and Bilge Yildiz[1, 2, *]

[1] Laboratory for Electrochemical Interfaces, Department of Nuclear Science and Engineering, Massachusetts Institute of Technology, 77 Massachusetts Avenue, Cambridge, MA, USA, 02139.
[2] Department of Materials Science and Engineering, Massachusetts Institute of Technology, 77 Massachusetts Avenue, Cambridge, MA, USA, 02139.
[*] E-mail: byildiz@mit.edu

Keywords: extended defect, dislocation, point defect chemistry, segregation

Abstract: Stabilizing atomically dispersed catalytic metal species at surfaces is a significant challenge for obtaining high-performance single-atom catalysts. This is because of the strong tendency for the dispersed metal atoms to agglomerate. We propose that dislocations can provide a strong anchor for stabilizing single atoms. A ½<110>{100} edge dislocation in Cu doped ceria, Cu-CeO₂, is investigated as a model system with density functional theory. The defect formation energies are found to be lower at the dislocation core, with a large segregation energy ranging within 0.8 – 2.5 eV depending on the site and species at dislocation core. The high segregation energy indicates that the edge dislocations can enrich Cu defects in an atomically-sized area, and thus, have a potential to strongly anchor single atom species at surfaces. Moreover, the edge dislocation also stabilizes reduced cation species, Cu (1+) and Ce (3+). The more reduced dislocation core can offer high concentration of oxygen vacancy as well as in-gap electronic states which provide more reactivity for surface reactions.

I. Introduction

Loading ceria with transition metal and noble metal nanoparticles, such as Cu, Pt and Au, can greatly enhance the catalytic performance of ceria for low temperature water gas shift reactions (WGS) and reforming of hydrocarbons [1–9]. The efficiency of ceria-based catalysts can be enhanced by precise control of the morphology of the metal addition at the surface of ceria. Flytzani-Stephanopoulos and Gates have shown that the catalytic activity of ceria-gold composite for low temperature water gas shift reactions is enhanced only with atomically dispersed gold on ceria surfaces, not by gold particles that consist of more than one atom [2,10,11]. However, most single-atom catalysts lose their activity after operating at elevated temperatures or in reducing environments [12,13] since the single-atom metal species agglomerate and form larger nanoparticles.

Here, we propose to use the undercoordinated surface terminations of dislocations for anchoring single atom catalysts. It is known that undercoordinated surface sites, such as vacancies or step edges can anchor single atom metal particles [14–16]. For example, Wan et al. showed that surface vacancies on TiO_2 can anchor single Au atoms and promote CO oxidation [17]. Surface vacancies are mobile species at high temperature, and can diffuse and assist the agglomeration of single Au atoms [18,19]. Extended defects can be a better anchor because they are much more stable than oxygen vacancies. In fact, Jones et al. [16] has found that a high density of surface steps on polyhedral-shaped nanoparticles can anchor a high concentration of atomically dispersed Pt and thus have better catalytic activity. We believe this approach is still prone to migration and agglomeration of single atoms *along* the step edges. Alternatively, dislocations can have a strong anchoring effect due to their undercoordinated surface terminations and their immobile nature. Dislocations in Al_2O_3 and MgO have been shown to localize dopant atoms at or near their core [20,21]. In addition, their core size at surface terminations is only of atomic dimensions, not allowing for agglomeration at low concentrations of single atoms at the surface. Furthermore, a

2

high density of dislocations can be achieved in nanoparticles of ceria by ball milling [22], ion radiation [23,24] , and controlling the growth conditions [25–28].

In this work, we take Cu catalyst atoms in CeO_2 as a model system, and assess whether Cu prefers to segregate to the dislocation, how strong the segregation can be, and the potential changes in oxidation state of the catalyst and the host at the dislocation core. $Cu-CeO_2$ is chosen as a model system because the bulk defect chemistry of $Cu-CeO_2$ without dislocations is well studied in our previous work [29]. More importantly, $Cu-CeO_2$ is a promising catalyst; it is equivalent to or even outperforms $Au-CeO_2$ and $Pt-CeO_2$ for water gas shift reactions [1,30,31].

In order to theoretically quantify the anchoring effect, a ½ <110>{100} edge dislocation model is taken to compute the defect formation energy in CeO_2 using density functional theory with Hubbard U corrections (DFT+U). The calculations here are performed in a model of dislocation in the bulk of ceria. We assume that the findings can be extrapolated to the surface terminations of dislocations because the dislocation has a similar core structure in the bulk and at the surface, and similar extended strain-stress fields [32]. Therefore, the Cu defect segregation energy to dislocation in bulk ceria can serve as an estimator for Cu segregation to the dislocation termination at surfaces.

II. Computational methods

The simulation is performed with the Vienna ab initio simulation package (VASP) [33–35], version 5.4.1. Generalized gradient approximation (GGA) with the Perdew-Wang 91(PW91) exchange correlation functional [36] is used. The cerium, oxygen and copper atoms are simulated with valence electrons of $5s^25p^66s^25d^14f^1$, $2s^22p^6$, and $3p^63d^{10}4p^1$, respectively. In each calculation, the ion positions are optimized by conjugate-gradient algorithm with only gamma

point and 400 eV energy cutoff until the force on each atom is smaller than 0.01 eV/Å. The final energy is then computed with a $1\times4\times1$ k-point mesh and 450 eV energy cutoff. Hubbard U corrections are applied to Ce f orbitals and Cu d orbitals with $U_{Ce} = 5$ eV and $U_{Cu} = 4$ eV.

An ½<110>{100} edge dislocation is simulated in this work. The initial configuration of the dislocation is constructed by Atomsk, an crystal structure tool-kit [37]. The edge dislocation is introduced by removing half {110} lattice plane at the lower half of the super cell and displacing the remaining atoms according to the elastic displacement field of an isolated edge dislocation. The simulation cell is periodic along all three directions and one O-Ce-O tri-layer at the boundary of the simulation cell is fixed during all calculations. Similar set up has been used for SrTiO$_3$ and MgSiO$_3$ dislocations [38]. The pristine dislocation configuration contains 612 atoms, with a cell size of 33Å×7.8Å ×33Å.

The defect formation energy is computed by subtracting the energy of the perfect cell ($E_{perfect}^{DFT+U}$) from the defected cell (E_{defect}^{DFT+U}) and adding chemical potential terms and correction terms. For charged defects, Makov-Payne correction [39] was applied. The resulting correction is on the order of 10^{-2} eV, negligible compared to defect formation energies at the dislocation core. Details of the point defect calculations can be found in our previous work on bulk Cu-CeO$_2$ defect chemistry [29].

III. Results and Discussion

A. Atomic and electronic structure of the edge dislocation

The relaxed structure of the ½ <110>{100} edge dislocation is shown in **FIG 1**a. This dislocation core is charge neutral, with a pentagonal shape of core structure. The core region includes five columns of Ce ions and 14 columns of O ions, shown in Fig. 1a-inset. The local strain tensor of this relaxed structure can be computed using the Ce-O bond distances and bond angles (details see Supplementary Materials [40]). The *xx* element of the strain tensor, e_{xx}, and the shear invariant, η_s, are shown in FIG 1b and c. Away from the dislocation, the strain field is consistent with the elastic theory (shown in **Fig. S1** [40]), with a uniaxial compressive strain, $\varepsilon_{xx} = -3\%$, at plane 14-20 and uniaxial tensile strain, $\varepsilon_{xx} = 3\%$, at plane 2-6. At the dislocation core, this DFT predicted strain is different from the elastic theory prediction due to the strong atomic displacements. At the tensile side of the dislocation core, an oxygen column (marked as 9D in FIG 1a-inset) splits into two columns, each of them being half occupied. At the glide plane, 10B and 10F columns also slightly split. As a result of these displacements, the local bond distances can be stretched or compressed by up to 10% (FIG 1b). This change in bond length is much higher than the strain predicted by the elastic theory. Apart from the change in bond distances, a strong distortion of bond angles is also observed at the dislocation core. The DFT predicted shear invariant (FIG 1c), which reflects the lattice distortion, spreads along the glide plane further than the elastic theory prediction (Fig. S1 [40]).

The electronic structure at the dislocation core is also different from bulk ceria. Fig. 1d shows that compared to dislocation-free ceria, the valence band maximum shifts up by 0.2 eV while the conduction band minimum shifts down by 0.2 eV. These shifts eventually lead to a band gap of E_g=1.9 eV at the dislocation, that is 0.4 eV smaller than band gap $E_{g, bulk}$=2.3 eV in bulk ceria.
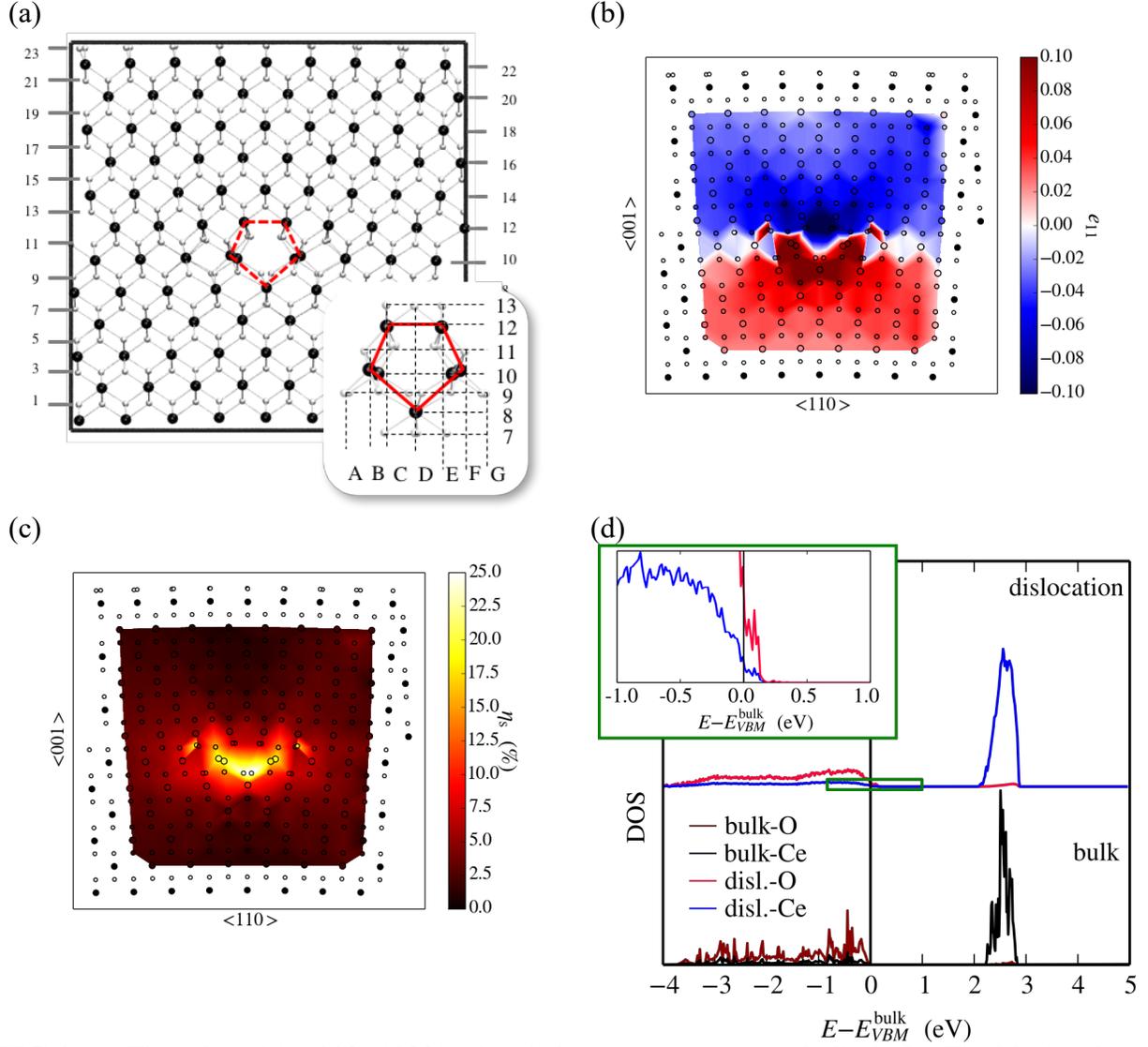
FIG 1. (a) The relaxed ½<110>{100} edge dislocation structure in bulk CeO₂. The black spheres represent Ce ions while the white spheres represent O ions. (b)The *xx* element of strain tensor, e_{xx}. (c) The shear invariant of the local strain, η_s. (d) The partial density of states (PDOS) for Ce ions (blue) and O ions (red) that are within 8.5 Å from the dislocation core, compared to bulk DOS. The inset zooms in on the -1 eV to 1 eV range for the dislocation PDOS. The bulk DOS is also plotted for comparison.

B. Defect enrichment region confined to atomic dimensions at the dislocation core

The lattice distortions and atom displacements around the edge dislocation, in particular at the core or in its vicinity, can affect the local defect formation energy by facilitating bond breaking and lattice relaxation. Here, we investigate several dominant Cu defect species and intrinsic defects that are found in bulk ceria. The defects include Cu substitutions with 1+ to 3+ oxidation states (Cu'_{Ce}, Cu''_{Ce}, and Cu'''_{Ce}), Cu interstitials ($Cu^{\bullet}_i$ and $Cu^{\bullet\bullet}_i$), and oxygen vacancies ($V^{\bullet\bullet}_O$). In addition, two defect complexes are also computed. One contains a substitution and a vacancy ($Cu''_{Ce} - V^{\bullet\bullet}_O)^{\times}$ and the other one contains a polaron and an interstitial ($Ce'_{Ce} - Cu^{\bullet}_i)^{\times}$. The segregation energy of these defects can then be computed by,

$$E_{seg} = -E_f^{disl} + E_f^{bulk},\tag{1}$$

where E_f^{disl} is the defect formation energy at the dislocation core and E_f^{bulk} is that in the bulk as a reference.

First, the formation energies of $V^{\bullet\bullet}_O$ and $(Cu''_{Ce} - V^{\bullet\bullet}_O)^{\times}$ at different sites adjacent to the dislocations are assessed and plotted in **FIG 2**. More than 10 locations were assessed for both defects, marked as the red and blue sites in Fig. 2a and 2c. For $V^{\bullet\bullet}_O$, three low energy sites are found at the tensile side, marked as D7, D9 and C7 in FIG 2a. These three sites have a low vacancy formation energy because of the longer Ce-O bond distances (4% longer than the bulk bonds) and significant lattice distortion (equivalent to 10% shear strain). These three sites are immediately next to each other, which means it is easy for a vacancy to hop among these sites. However, these sites confine vacancies locally to the dislocation core since the formation energies away from the

dislocation are higher. For example, it takes at least 0.9 eV for a vacancy to hop from site D9 to the adjacent site A9.
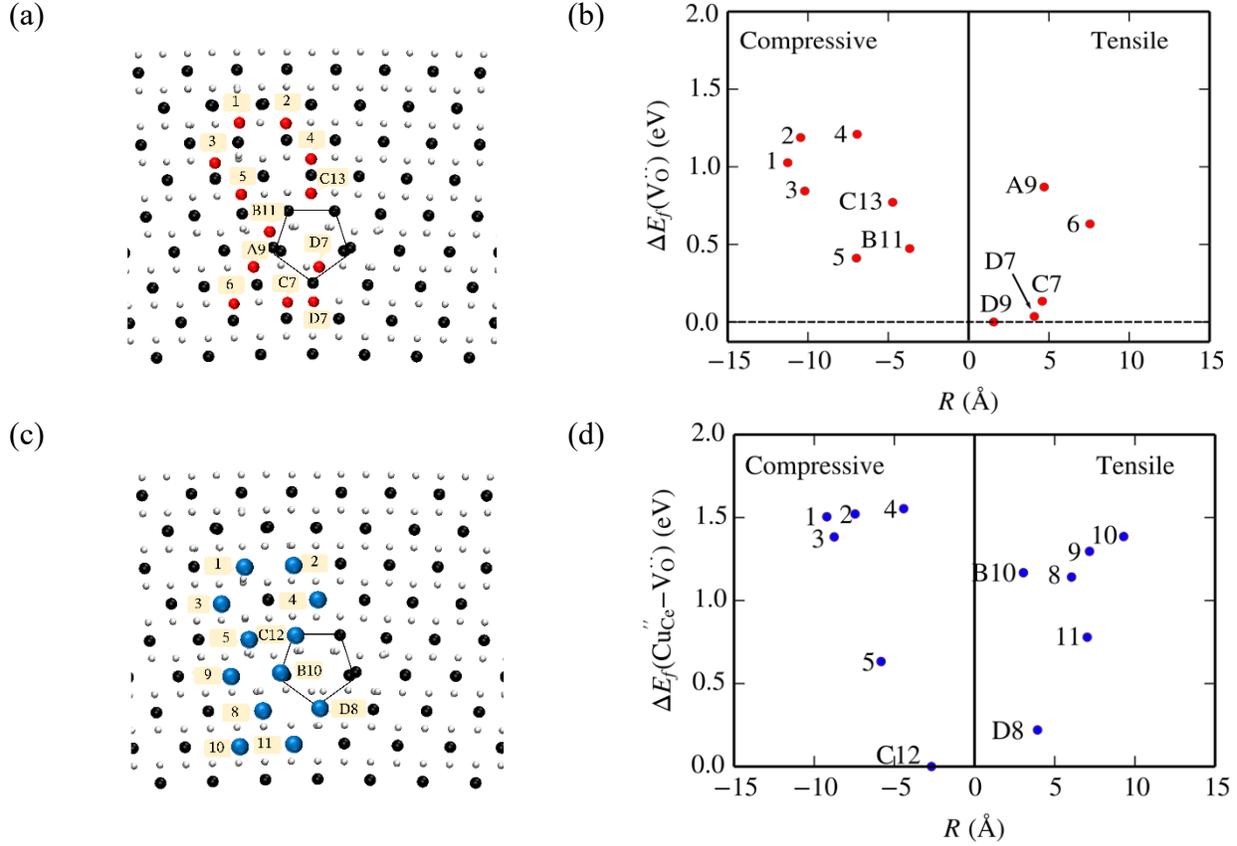
FIG 2. (a) Map of sites, marked by red spheres, where the $V_O^{\bullet\bullet}$ formation energies were computed. (b) Relative defect formation energy of a $V_O^{\bullet\bullet}$ defect complex as a function of its distance, R, to the dislocation core. (c) Map of sites, marked by blue spheres, where the $(Cu_{Ce}'' - V_O^{\bullet\bullet})^\times$ formation energies were computed. (d) Relative defect formation energy of a $(Cu_{Ce}'' - V_O^{\bullet\bullet})^\times$ defect complex as a function of its distance, R, to the dislocation core. The black and white spheres in (a) and (c) represent Ce and O ions, respectively.

Unlike $V_O^{\bullet\bullet}$, the lowest defect formation energy for $(Cu_{Ce}'' - V_O^{\bullet\bullet})^\times$ is found at the compressive side, C12. The second lowest formation energy is found at the tensile side D8, whose formation energy is 0.2 eV higher than the one at site C12. These two sites attract $(Cu_{Ce}'' - V_O^{\bullet\bullet})^\times$ due to the

local lattice distortion. In bulk ceria, the Cu^{2+} substitution and its neighbor oxygen sites are displaced to form a lower energy configuration with either square-planar coordination or tetragonal coordination. At these two sites (C12 and D8) around the dislocation, these coordination environments can easily form without displacing the Cu or oxygen atoms. All the remaining sites have formation energies $0.6 - 1.5$ eV higher than C12.

Both $V_O^{\bullet\bullet}$ and $(Cu_{Ce}'' - V_O^{\bullet\bullet})^{\times}$ have a formation energy substantially lower than the bulk at the dislocation core, indicating a strong enrichment effect. More importantly, these preferential, low formation energy zones are limited at two to three atom sites right next to the dislocation core.

Next, formation energies for the remaining Cu-related defects at the dislocation core are computed. The relaxed configurations and the spin state contours of these defects are plotted in **FIG 3**.

The segregation energies for oxygen vacancy and Cu related defects are all listed **TABLE I**. All segregation energies are positive and on the order of 1-2 eV. Generally, the larger the defect, the more sensitive it is to the difference between the dislocation core and the bulk, and thus a larger segregation energy. $(Ce_{Ce}' - Cu_i^{\bullet})^{\times}$ has the highest segregation energy, followed by $Cu_i^{\bullet}$ and $Cu_i^{\bullet\bullet}$, while $Cu_i^{\bullet\bullet\bullet}$ has the lowest segregation energy. This is because $Cu_i^{\bullet}$ have a larger Shannon radius than that of $Cu_i^{\bullet\bullet}$ and $Cu_i^{\bullet\bullet\bullet}$; a $(Ce_{Ce}' - Cu_i^{\bullet})^{\times}$ has an even larger relaxation volume than other interstitial defects since the defect complex has a Ce^{3+} (whose Shannon radius is larger than Ce^{4+}) and a $Cu_i^{\bullet}$.
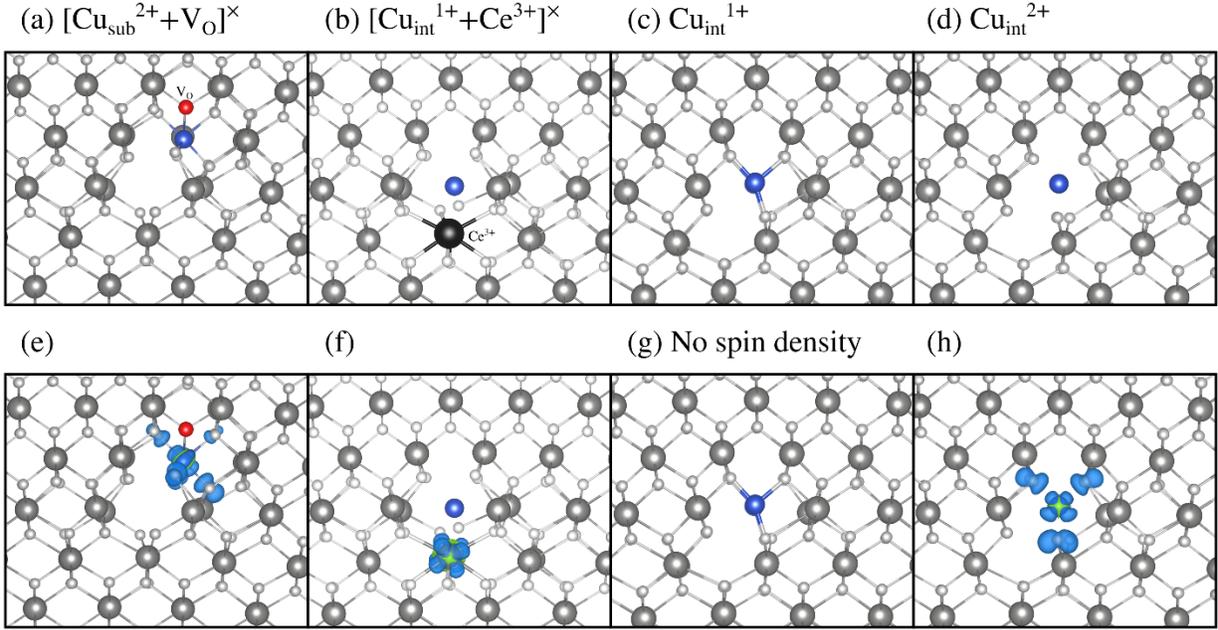
FIG 3. Lowest energy configurations (a-d) and their spin density contours (e-h) for Cu defects at the ½ <110>{100} edge dislocation core in bulk CeO_2. In g, there is no spin density since Cu^{1+} is a closed shell ion.

TABLE I. Segregation energies, E_{seg}, for different Cu defects.

Defect	Segregation Energy (eV)	Defect	Segregation Energy (eV)
$Cu_i^{\bullet}$	2.0	$V_O^{\bullet\bullet}$	1.3
$Cu_i^{\bullet\bullet}$	1.4	$(Ce_{Ce}' - V_O^{\bullet\bullet} - Ce_{Ce}')^{\times}$	1.0
$Cu_i^{\bullet\bullet\bullet}$	0.8	$(V_O^{\bullet\bullet} - Cu_{Ce}'')^{\times}$	1.2
Cu_{Ce}'	1.2	$(Ce_{Ce}' - Cu_i^{\bullet})^{\times}$	2.5
Cu_{Ce}''	1.9		

C. Preferential segregation of defects with lower oxidation state

10

The large positive segregation energy indicates that all defect species enrich at the dislocation, but some have higher concentrations than others. In **FIG 4**, the formation energies of different defects are plotted as a function P_{O_2} and electron chemical potential μ_e. Under oxygen rich conditions, $P_{O_2} = 1\ bar$, the equilibrium bulk Fermi level is 0.54 eV. At this Fermi level, bulk $V_O^{\bullet\bullet}$ have the lowest formation energy, around 1.5 eV, close to Cu'_{Ce}. Therefore, bulk ceria without dislocations have Cu'_{Ce} and $V_O^{\bullet\bullet}$ as dominant defects. In dislocations, the dominant defects are Cu''_{Ce} and $V_O^{\bullet\bullet}$ with formation energies close to zero. The Cu oxidation state is lower in dislocation core than in the bulk.

Under oxygen poor conditions, $P_{O_2} = 10^{-20}$ bar, the bulk Fermi level is around 1.29 eV. At this Fermi level, both dislocations and bulk have $Cu_i^{\bullet}$ and $V_O^{\bullet\bullet}$ as dominant defects. These two positively charged species are charge compensated by the negative defects with the lowest formation energy. In bulk ceria, the charge compensating species is Ce'_{Ce}. At dislocation core, $(Ce'_{Ce} - V_O^{\bullet\bullet} - Ce'_{Ce})^{\times}$ and $(Ce'_{Ce} - Cu_i^{\bullet})^{\times}$ have lower formation energy than those of all other Cu substitutional defects (see Fig. 4d). Therefore, the charge compensating species at the dislocation core is also Ce'_{Ce}.

Compared to bulk ceria, the dislocation stabilizes the lower oxidation states of Cu, which can be demonstrated by the formation energy difference between a Cu^{1+} defect and a Cu^{2+} defect, for example, $E_{Cu_i^{\bullet\bullet}} - E_{Cu_i^{\bullet}}$ and $E_{Cu''_{Ce}-V_O^{\bullet\bullet}} - E_{Cu_i^{\bullet}}$. These energy differences are listed in Table II. For the energy difference between $Cu_i^{\bullet}$ and $Cu_i^{\bullet\bullet}$, $E_{Cu_i^{\bullet\bullet}} - E_{Cu_i^{\bullet}}$ at all conditions is larger than zero, which means the $Cu_i^{\bullet}$ is always easier to form than $Cu_i^{\bullet\bullet}$. In dislocation free ceria, $E_{Cu_i^{\bullet\bullet}} - E_{Cu_i^{\bullet}}$ is only 0.08eV when $P_{O_2} = 1$ bar. This small difference means that it is feasible to oxidize a $Cu_i^{\bullet}$ to $Cu_i^{\bullet\bullet}$ at oxygen rich environments. However, at the dislocation core, this energy difference is much higher. It takes 0.8 eV to convert a $Cu_i^{\bullet}$ to $Cu_i^{\bullet\bullet}$, meaning that it is hard to oxidize $Cu_i^{\bullet}$ at the

dislocation core. Similarly, the energy difference between $(Cu''_{Ce} - V_O^{\bullet\bullet})^\times$ (where Cu is 2+) and

$Cu_i^\bullet$, $(E_{Cu''_{Ce}-V_O^{\bullet\bullet}} - E_{Cu_i^\bullet})$, is higher at the dislocation core, which indicates it is harder to convert

$Cu_i^\bullet$ to $(Cu''_{Ce} - V_O^{\bullet\bullet})^\times$ at the dislocation core than in the bulk.
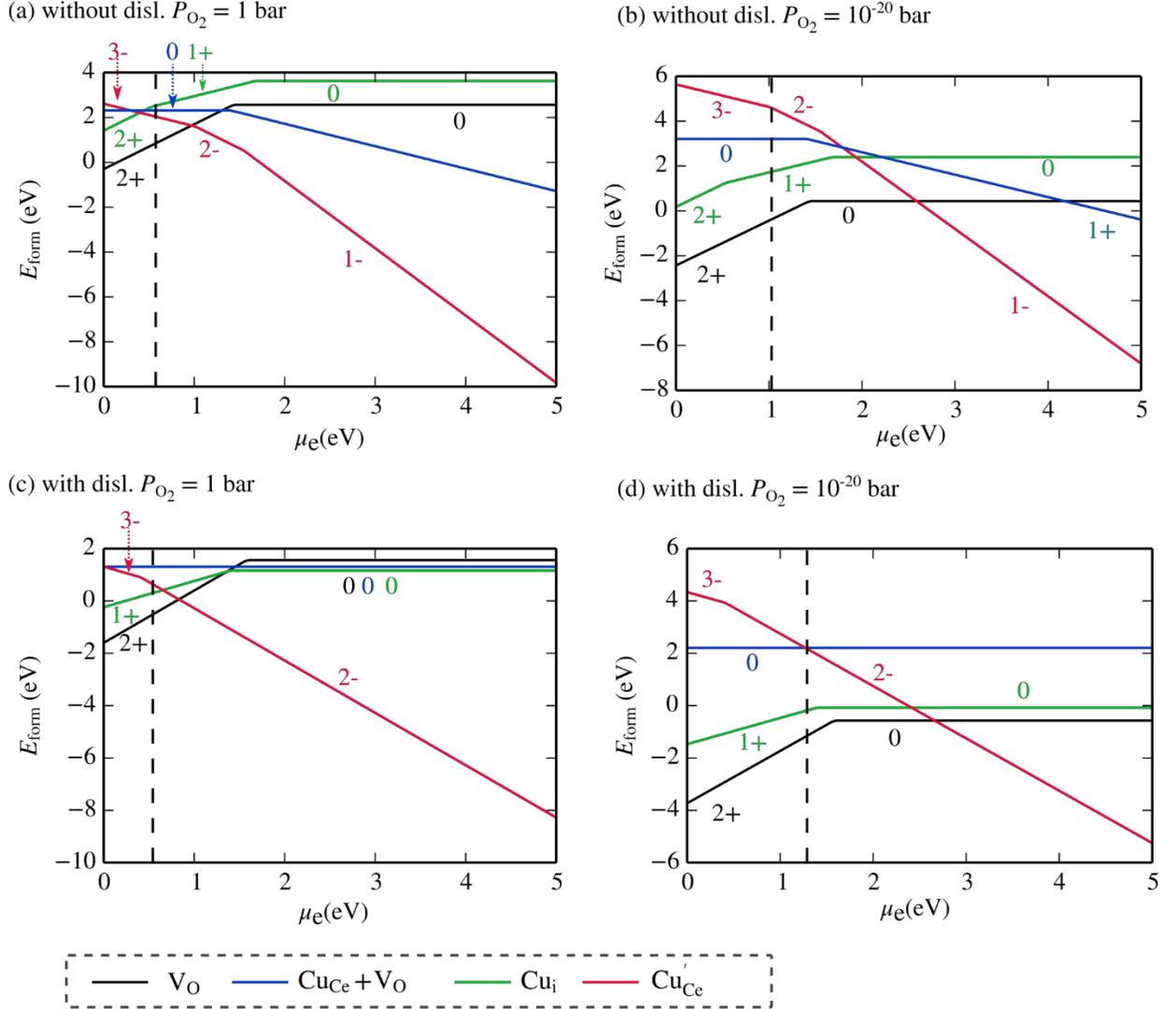
FIG 4. Defect formation energy as a function of electron chemical potential, E_{Fermi}, for ceria (a) without dislocations, $P_{O_2} = 1$ bar, (b) without dislocations, $P_{O_2} = 10^{-20}$ bar, (c) with dislocations, $P_{O_2} = 1$ bar, (d) with dislocations, $P_{O_2} = 10^{-20}$ bar. The effective charge state of each defect is labeled on the plot.

TABLE II. The energy needed to convert Cu^{1+} to Cu^{2+} (the first two columns of energies), and to form a Ce^{3+} next to Cu^{1+} interstitials (last column) at different P_{O_2} conditions. Unit: eV.

P_{O_2} (bar)	E_F (eV)	$E_{Cu_i^{\bullet\bullet}} - E_{Cu_i^\bullet}$	$E_{Cu_i^\bullet - Ce'_{Ce}} - E_{Cu_i^\bullet}$	$E_{Cu''_{Ce} - V_O^{\bullet\bullet}} - E_{Cu_i^\bullet}$
		Dislocation-free		
1	0.54	0.08	1.13	-0.90
10^{-20}	1.29	0.83	0.39	0.53
		Dislocation-core		
1	0.54	0.80	0.85	0.34
10^{-20}	1.29	1.55	0.11	1.72

Dislocations stabilize not only the more reduced Cu oxidation state, but also the reduced cerium cations Ce^{3+}. The formation energy difference between $(Ce'_{Ce} - Cu_i^\bullet)^\times$ and $Cu_i^\bullet$ is lower at the dislocation core than in bulk ceria. This result indicates that it is easier to form a Ce^{3+} adjacent to a $Cu_i^\bullet$ at dislocation cores.

Given the large positive segregation energies, the core of dislocations can enrich Cu defects by many orders of magnitude. For example, the concentration of $Cu_i^\bullet$ at dislocation cores can be at least $e^{\frac{1.3\ eV}{k_B T}} = 4.8 \times 10^9$ times higher than the bulk concentration at 400 °C. More importantly, the 10^9 times higher defect concentration region is limited only to several atomic sites at the dislocation core. Away from this several sites, the segregation energies decay rapidly, and the defect concentration is high away from the dislocation. This leads to a very *localized atomic scale* enrichment of the Cu. The contribution of these few enrichment sites to the overall bulk-average defect concentration may be limited, but they greatly impact the size of Cu cluster that can form at dislocation terminations at the surface. At Cu areal concentrations lower than the concentration of dislocation terminations, and in the absence of any other trap sites, the only place that Cu atoms can go to are the dislocations at the surface. And because the energy difference to get out of those

dislocation sites is very high (at least 0.6 eV for the Cu to hop out of these trap sites), this configuration should avoid Cu metal out-diffusion and agglomeration to form larger clusters. This gives dislocations a good potential to stabilize and anchor atomically dispersed Cu metal species.

If the Cu concentration is higher than the dislocation concentration, the dislocation core terminated at the surface can collect more than one single Cu atom, and a lot more can accumulate along the dislocations into the depths of ceria. Therefore, the Cu areal concentration needs not exceed the dislocation density, which is about $0.06/nm^2$ (assuming the inter-dislocation distance is 4 nm [27,32,41]).

The strong distortion and displacement of atoms at the dislocation core not only changes the defect concentration, but also their preferred oxidation states. For Cu interstitials and substitutions, the dislocation offers more space to relax the defect configurations. The larger the defect, the more it benefits from the dislocation's open space. For this reason, the Cu^{1+} interstitials have a larger segregation energy than 2+ or 3+ interstitials. It is easier to have Cu^{1+} at the dislocation core than the bulk without dislocations. Ce^{3+} is also found to be more stable at dislocation core for two reasons. On one hand, dislocation cores offer open space to facility the formation of Ce^{3+}. On the other hand, dislocations enrich Cu_i and $V_O^{\bullet\bullet}$ at oxygen poor conditions, which can raise Ce^{3+} concentration to charge compensate these positive defects.

The enrichment of Cu^{1+} interstitials and Ce^{3+} at the dislocation core are beneficial for the surface reactivity [42] since they introduce in-gap electronic states higher than the bulk valence band maximum [43]. These in-gap states are essentially excess charge localized on cation, which can enhance local catalytic activity. For example, the excess charge at the surface of anatase is known to improve O_2 adsorption [44] and water dissociation [45]. The reduced Cu interstitials and reduced host cations at the dislocation core are accompanied by a high concentration of oxygen

14

vacancies as well. The oxygen vacancy has a large segregation energy since the tensile strain around the dislocation eases the bond breaking for vacancy formation. These oxygen vacancies can reduce the reaction barrier of water dissociation and hence improve surface activity [46–48].

IV. Conclusion

In summary, the ½ <110>{100} edge dislocation introduces significant distortion and displacement of atomic positions at and near the dislocation core. The core structure alters the local electronic structure as well as defect formation energy. Several atomic sites at the dislocation core are found to have the lowest $V_O^{\bullet\bullet}$ and $(Cu''_{Ce} - V_O^{\bullet\bullet})^{\times}$ formation energy. This means that dislocation cores can trap point defect or Cu species at 2-3 atom sites, indicating a good anchoring effect for single atom catalysts at the surface termination of the dislocation. The segregation energy of Cu_i, Cu_{Ce} and $V_O^{\bullet\bullet}$ ranges within $0.8 - 2.5$ eV. The Cu^{1+} and Ce^{3+} ions are more stable at dislocation core in contrast to those in the bulk without dislocations. The more reduced dislocation core can offer high concentration of oxygen vacancies as well as in-gap states, which enable a more highly reactive surface for water gas shift reactions.

Supplementary Materials: The DFT- and elastic-theory-predicted strain tensor maps for all components around the dislocation, partial density of states per atomic plane for the dislocation, the effect of strain on density of states for bulk ceria.

Notes The authors declare no competing financial interest.

15

References

[1] A. Trovarelli and P. Fornasiero, editors , *Catalysis by Ceria and Related Materials*, 2nd edition (Imperial College Press, London, 2013).
[2] Q. Fu, H. Saltsburg, and M. Flytzani-Stephanopoulos, Science **301**, 935 (2003).
[3] Y. Liu, T. Hayakawa, K. Suzuki, S. Hamakawa, T. Tsunoda, T. Ishii, and M. Kumagai, Appl. Catal. Gen. **223**, 137 (2002).
[4] Y. Li, Q. Fu, and M. Flytzani-Stephanopoulos, Appl. Catal. B Environ. **27**, 179 (2000).
[5] G. Jacobs, U. M. Graham, E. Chenu, P. M. Patterson, A. Dozier, and B. H. Davis, J. Catal. **229**, 499 (2005).
[6] G. Jacobs, L. Williams, U. Graham, G. A. Thomas, D. E. Sparks, and B. H. Davis, Appl. Catal. Gen. **252**, 107 (2003).
[7] J. Paier, C. Penschke, and J. Sauer, Chem. Rev. **113**, 3949 (2013).
[8] W. C. Chueh, Y. Hao, W. Jung, and S. M. Haile, Nat. Mater. **11**, 155 (2012).
[9] L. Malavasi, C. A. J. Fisher, and M. S. Islam, Chem. Soc. Rev. **39**, 4370 (2010).
[10] M. Flytzani-Stephanopoulos and B. C. Gates, Annu. Rev. Chem. Biomol. Eng. **3**, 545 (2012).
[11] R. Si and M. Flytzani-Stephanopoulos, Angew. Chem. **120**, 2926 (2008).
[12] Y. Chen, S. Ji, C. Chen, Q. Peng, D. Wang, and Y. Li, Joule **2**, 1242 (2018).
[13] R. Bliem, J. E. S. van der Hoeven, J. Hulva, J. Pavelec, O. Gamba, P. E. de Jongh, M. Schmid, P. Blaha, U. Diebold, and G. S. Parkinson, Proc. Natl. Acad. Sci. **113**, 8921 (2016).
[14] F. Dvořák, M. Farnesi Camellone, A. Tovt, N.-D. Tran, F. R. Negreiros, M. Vorokhta, T. Skála, I. Matolínová, J. Mysliveček, V. Matolín, and S. Fabris, Nat. Commun. **7**, 10801 (2016).
[15] A. Figueroba, G. Kovács, A. Bruix, and K. M. Neyman, Catal Sci Technol (2016).
[16] J. Jones, H. Xiong, A. T. DeLaRiva, E. J. Peterson, H. Pham, S. R. Challa, G. Qi, S. Oh, M. H. Wiebenga, X. I. P. Hernández, Y. Wang, and A. K. Datye, Science **353**, 150 (2016).
[17] J. Wan, W. Chen, C. Jia, L. Zheng, J. Dong, X. Zheng, Y. Wang, W. Yan, C. Chen, Q. Peng, D. Wang, and Y. Li, Adv. Mater. **30**, 1705369 (2018).
[18] S. Lee, C. Fan, T. Wu, and S. L. Anderson, Surf. Sci. **578**, 5 (2005).
[19] M. H. Jang, R. Agarwal, P. Nukala, D. Choi, A. T. C. Johnson, I.-W. Chen, and R. Agarwal, Nano Lett. **16**, 2139 (2016).
[20] K. P. McKenna, J. Am. Chem. Soc. **135**, 18859 (2013).
[21] A. Nakamura, K. Matsunaga, J. Tohma, T. Yamamoto, and Y. Ikuhara, Nat. Mater. **2**, 453 (2003).
[22] R. Sen, S. Das, and K. Das, Metall. Mater. Trans. A **42**, 1409 (2011).
[23] A. Kumar, R. Devanathan, V. Shutthanandan, S. V. N. T. Kuchibhatla, A. S. Karakoti, Y. Yong, S. Thevuthasan, and S. Seal, J. Phys. Chem. C **116**, 361 (2012).

[24] P. D. Edmondson, Y. Zhang, S. Moll, F. Namavar, and W. J. Weber, Acta Mater. **60**, 5408 (2012).

[25] A. C. Johnston-Peck, S. D. Senanayake, J. J. Plata, S. Kundu, W. Xu, L. Barrio, J. Graciani, J. F. Sanz, R. M. Navarro, J. L. G. Fierro, E. A. Stach, and J. A. Rodriguez, J. Phys. Chem. C **117**, 14463 (2013).

[26] C.-C. Chen, C. Zhu, E. R. White, C.-Y. Chiu, M. C. Scott, B. C. Regan, L. D. Marks, Y. Huang, and J. Miao, Nature **496**, 74 (2013).

[27] T. X. T. Sayle, B. J. Inkson, A. Karakoti, A. Kumar, M. Molinari, G. Möbus, S. C. Parker, S. Seal, and D. C. Sayle, Nanoscale **3**, 1823 (2011).

[28] R. Si, J. Raitano, N. Yi, L. Zhang, S.-W. Chan, and M. Flytzani-Stephanopoulos, Catal. Today **180**, 68 (2012).

[29] L. Sun and B. Yildiz, J. Phys. Chem. C (2018).

[30] J. A. Rodriguez, P. Liu, J. Hrbek, J. Evans, and M. Pérez, Angew. Chem. Int. Ed. **46**, 1329 (2007).

[31] M. M. Branda, N. C. Hernández, J. F. Sanz, and F. Illas, J. Phys. Chem. C **114**, 1934 (2010).

[32] H. Hojo, E. Tochigi, T. Mizoguchi, H. Ohta, N. Shibata, B. Feng, and Y. Ikuhara, Appl. Phys. Lett. **98**, 153104 (2011).

[33] G. Kresse and D. Joubert, Phys. Rev. B **59**, 1758 (1999).

[34] G. Kresse and J. Hafner, Phys. Rev. B **47**, 558 (1993).

[35] G. Kresse and J. Hafner, Phys. Rev. B **49**, 14251 (1994).

[36] J. P. Perdew and Y. Wang, Phys. Rev. B **45**, 13244 (1992).

[37] P. Hirel, A. Kraych, P. Carrez, and P. Cordier, Acta Mater. **79**, 117 (2014).

[38] P. Hirel, M. Mrovec, and C. Elsässer, Acta Mater. **60**, 329 (2012).

[39] G. Makov and M. C. Payne, Phys. Rev. B **51**, 4014 (1995).

[40] See Supplemental Material at [URL] for the DFT- and elastic-theory-predicted strain tensor maps for all components around the dislocation, partial density of states per atomic plane for the dislocation, the effect of strain on density of states for bulk ceria.

[41] Z.-P. Li, T. Mori, F. Ye, D. R. Ou, J. Zou, and J. Drennan, Microsc. Microanal. **17**, 49 (2011).

[42] Z. Yang, L. Xie, D. Ma, and G. Wang, J. Phys. Chem. C **115**, 6730 (2011).

[43] D. Marrocchelli, S. R. Bishop, H. L. Tuller, and B. Yildiz, Adv. Funct. Mater. **22**, 1958 (2012).

[44] M. Setvin, B. Daniel, U. Aschauer, W. Hou, Y.-F. Li, M. Schmid, A. Selloni, and U. Diebold, Phys. Chem. Chem. Phys. **16**, 21524 (2014).

[45] S. Selcuk and A. Selloni, Nat. Mater. **15**, 1107 (2016).

[46] X. Wang, J. A. Rodriguez, J. C. Hanson, D. Gamarra, A. Martínez-Arias, and M. Fernández-García, J. Phys. Chem. B **110**, 428 (2006).

[47] M. Molinari, S. C. Parker, D. C. Sayle, and M. S. Islam, J. Phys. Chem. C **116**, 7073 (2012).

[48] J. A. Rodriguez, S. Ma, P. Liu, J. Hrbek, J. Evans, and M. Pérez, Science **318**, 1757 (2007).